Refinement and Coarsening Indicators for Adaptive Parameterization: Application to the Estimation of Hydraulic Transmissivities

Hend Ben Ameur, Guy Chavent, Jérôme Jaffré

INRIA

INSTITUT NATIONAL DE RECHERCHE EN INFORMATIQUE ET EN AUTOMATIQUE

Refinement and coarsening indicators for adaptive parameterization: application to the estimation of hydraulic transmissivities

Hend Ben Ameur — Guy Chavent — Jérôme Jaffré

N° 4292

Octobre 2001

THÈME 4

ISSN 0249-6399 ISRN INRIA/RR--4292--FR+ENG

INRIA
ROCQUENCOURT

Refinement and coarsening indicators for adaptive parameterization: application to the estimation of hydraulic transmissivities

Hend Ben Ameur* , Guy Chavent† , Jérôme Jaffré‡

Thème 4 — Simulation et optimisation
de systèmes complexes
Projets Estime

Rapport de recherche n° 4292 — Octobre 2001 — 27 pages

Abstract: When estimating hydraulic transmissivity the question of parameterization is of great importance. The transmissivity is assumed to be a piecewise constant space dependent function and the unknowns are both the transmissivity values and the zonation, the partition of the domain whose parts correspond to the zones where the transmissivity is constant. Refinement and coarsening indicators, which are easy to compute from the gradient of the least squares misfit function, are introduced to construct iteratively the zonation and to prevent overparameterization.

Key-words: Parameter estimation, adaptive parameterization, flow in porous media

* FSB, université Tunis II and ENIT-Lamsin, BP 37, Le Belvédère, Tunis, Tunisia, (Hend.Benameur@enit.rnu.tn)

† Inria-Rocquencourt and Ceremade, Université Paris-Dauphine, Place du Maréchal De Lattre de Tassigny, 75775 Paris Cedex 16, France, (Guy.Chavent@inria.fr)

‡ Inria-Rocquencourt, BP 105, 78153 Le Chesnay Cedex, France, (Jerome.Jaffre@inria.fr)

Unité de recherche INRIA Rocquencourt
Domaine de Voluceau, Rocquencourt, BP 105, 78153 Le Chesnay Cedex (France)
Téléphone : +33 1 39 63 55 11 —Télécopie : +33 1 39 63 53 30

Indicateurs de raffinement et déraffinement pour la paramtrisation adaptative: application à l'estimation de transmissivité hydraulique

Résumé : Dans l'estimation de transmissivités hydrauliques le choix de la paramétrisation joue un grand rôle. La transmissivité est ici supposée être une fonction constante par morceaux et les inconnues sont à la fois les valeurs de la transmissivité, ainsi que la zonation, c'est à dire la partition du domaine dont les parties sont les zones où la transmissivité est constante. Des indicateurs de raffinement et de déraffinement, faciles à calculer à partir du gradient de la fonction écart, sont introduits, permettant ainsi de construire itérativement la zonation tout en minimisant le nombre de paramètres.

Mots-clés : Estimation de paramètres, paramétrisation adaptative, écoulement en milieu poreux

1 Introduction

When estimating hydraulic transmissivities, which are space dependent coefficients in a parabolic partial differential equations, we minimize an objective function defined as a least-squares misfit between measurements and the corresponding quantities computed with a chosen parameterization of the transmissivities.

One of the difficulties in solving this problem is that, because of the high cost of experimental measurements, the data is usually insufficient to estimate the value of the hydraulic transmissivity in each cell of the computational grid. Therefore we have to find a parameterization of the transmissivity which reduces the number of unknowns. We refer to [Sun, 1994, Eppstein-Dougherty, 1996] for a presentation of the parameterizations which are the most commonly used in hydrogeology.

Lately multiscale parameterizations [Liu, 1993, Chavent-Liu, 1989] have provided a first answer to the problem of choosing the discretization of distributed parameters. With such an approach the parameter estimation problem is solved through successive approximations by refining the scale at which the transmissivities are described and the process is stopped when the refinement of the scale does not induce a significant decrease of the misfit function. This method has already brought interesting results in various problems of parameter estimation [Chardaire-Rivière et al., 1990, Chardighy et al., 1996]. However, when going from the current scale to a finer one, degrees of freedom are added uniformly in the domain of calculation, and so this approach can lead to overparameterization in the case where only a few local refinements are needed.

The method using refinement and coarsening indicators, that we present in this paper, tries to avoid such a drawback. At a given refinement level the parameters are estimated by minimizing the least-squares misfit to the data. Then we compute refinement and coarsening indicators which indicate the effect on the optimal data misfit of adding or removing some degrees of freedom and use these indicators to make a decision concerning the next refinement level. A variant of this method has already been presented in [Chavent-Bissel, 1998].

We apply this technique to the estimation of the distributed transmissivity parameter T in the partial differential equation

$$S\frac{\partial \Phi}{\partial t} + \text{div } (-T \text{ grad } \Phi) = Q \text{ in } \Omega, \tag{1}$$

where Ω is a domain in $\mathbb{R}^2$. This equation governs a two-dimensional groundwater flow in an isotropic and confined aquifer, subject to initial and boundary conditions

$$\begin{aligned} &\Phi = \Phi_d \text{ on } \Gamma_D, \quad (-T \text{ grad } \Phi) \cdot n = q_d \text{ on } \Gamma_N, \\ &\Phi(0) = \Phi_0 \text{ in } \Omega, \end{aligned} \tag{2}$$

where $\{\Gamma_D, \Gamma_N\}$ is a partition of the boundary of Ω supporting respectively Dirichlet and Neumann conditions and where

$\Phi =$ piezometric head,
$S(x,y) =$ storage coefficient,
$T(x,y) =$ hydraulic transmissivity,
$Q(x,y,t) =$ distributed source term,
Φ_d, q_d given boundary piezometric head and source terms,
$\Phi_0 =$ given initial piezometric head,
n is the unit normal vector to Ω.

The domain Ω is discretized with a mesh $\mathcal{T}$ and equations (1),(2) are approximated by a mixed-hybrid finite element method, which is suitable to the case where the parameter T have discontinuities [Chavent-Roberts, 1997].

Our problem is to search for a piecewise constant hydraulic transmissivity T. Both the zonation (the partition of Ω into zones where T is constant) and the value of T on each zone are to be determined and our aim is to be able to explain the data with a number of zones as small as possible.

We define our misfit function by

$$J(T) = \frac{1}{2} \sum_{i,j} |\Phi(T; x_j, t_i) - \Phi^m_{i,j}|^2, \tag{3}$$

where $\Phi^m_{i,j}$ is the piezometric head measured at point x_j at time t_i, and $\Phi(T; x_j, t_i)$ is the model output for current transmissivity values.

In order to have an iteration computational cost independent of the number of transmissivity values to estimate, we use the Quasi-Newton gradient algorithm (see [Bonnans et al., 1997]), which is known to be efficient in the case of a large number of unknown parameters. The gradient of J is computed by the adjoint state method [Chavent, 1974, Sun, 1994].

The code for the calculation of the piezometric head, the misfit function and its gradient has been obtained through automatic program generation [Jegou, 1997].

2 Refinement and coarsening indicators

Usually the data are insufficient to estimate the unknown parameter in each cell of the computing mesh $\mathcal{T}$. To every partition (zonation) $\mathcal{Z}$ of Ω, we associate hydraulic transmissivities T which are constant on each zone of $\mathcal{Z}$. In practice we suppose that the boundary of a zone in $\mathcal{Z}$ is made of edges or diagonals of cells of $\mathcal{T}$. The degrees of freedom of the transmissivity to be estimated are the values of the transmissivity in each zone of $\mathcal{Z}$. We want this number to be significantly lower than the number of elements in $\mathcal{T}$.

We introduce refinement and coarsening indicators in order to construct $\mathcal{Z}$ with the lowest possible number of zones. For this purpose, we need to define these indicators in such a way that, given a current parameterization, they will tell where to insert new discontinuities of the transmissivity and which ones can be removed.

2.1 Refinement indicators

We shall describe refinement indicators on an example. Let $(\mathcal{P}_1)$ be an initial problem where the hydraulic transmissivity is constant in all the domain (Figure 1(b)). So we have only one value of the transmissivity to estimate, which is done by minimizing the misfit function J with respect to this single variable. We denote by $(\mathcal{P}_2)$ the parameter estimation problem corresponding to a tentative partition of Ω into two zones Z_1 and Z_2 having different transmissivities (Figure 1(c)). We denote by $T^* = (T_1^*, T_2^*)$ the solution of $(\mathcal{P}_2)$ obtained by minimizing the misfit function with respect to the corresponding two variables. If $B = T_1^* - T_2^*$ were known, then the solution of minimizing J under the constraint $T_1 - T_2 = B$ is necessarily $T^* = (T_1^*, T_2^*)$, the solution of $(\mathcal{P}_2)$. But for $B = 0$ the $T = (T_0^*, T_0^*)$ solution of the corresponding constrained problem is obviously the solution of $(\mathcal{P}_1)$.

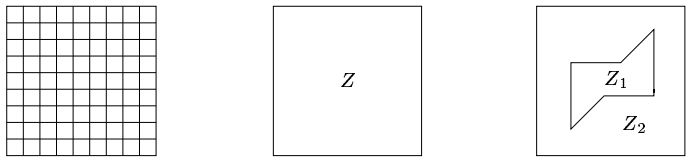

(a) Computing mesh $\mathcal{T}$

(b) Partition $\mathcal{Z}^1$ associated to problem $(\mathcal{P}_1)$

(c) Partition $\mathcal{Z}^2$ associated to problem $(\mathcal{P}_2)$

Figure 1: An example of parameterization refinement

To the problem of minimizing the misfit function under these constraints,

$$J(T^*) = \min_{AT=B} J(T),$$

we associate the Lagrangian function defined by

$$\mathcal{L}_B(T, \lambda) = J(T) - < \lambda, AT - B > \tag{4}$$

where λ is the Lagrange multiplier associated to the constraint $AT = B$. Then the Lagrange condition ensures that T^* satisfies

$$\begin{aligned} \frac{\partial \mathcal{L}_B}{\partial T}(T^*, \lambda^*) &= \nabla J(T^*) - A^T \lambda^* = 0, \\ \frac{\partial \mathcal{L}_B}{\partial \lambda}(T^*, \lambda^*) &= AT^* - B = 0. \end{aligned} \tag{5}$$

If we denote by $J_B^* = J(T^*) = \mathcal{L}_B(T^*, \lambda^*)$ the optimal misfit associated to the right hand side B of the constraint, we deduce from (4) and (5) that

$$\frac{\partial J_B^*}{\partial B}|_{B=0} = \frac{\partial \mathcal{L}_B}{\partial B}(T^*, \lambda^*)|_{B=0} = \lambda^*. \tag{6}$$

Therefore the Lagrange multiplier gives us the sensitivity of the optimal data misfit J_B^* to the perturbation B. For this reason we call λ^* a refinement indicator. It can be easily deduced from equation (5). In our example, the refinement indicator associated to splitting the single zone in Figure 1(b) into two zones in Figure 1(c) is

$$\lambda^* = \frac{\partial J}{\partial T_1}(T^*) = -\frac{\partial J}{\partial T_2}(T^*), \text{ where } T = (T_0^*, T_0^*). \tag{7}$$

Without solving $(\mathcal{P}_2)$, this indicator indicates through its absolute value, if the suggested refinement in Figure 1(c) is likely to induce an important decrease of the optimal misfit function.

One can see that we define such a refinement by introducing a curve (the boundary of Z_2 in Fig. 1(c)). We shall call such a curve a cut. It divides the domain into only two zones of different transmissivities. In practice, we will use only the families of cuts shown in Fig. 2.

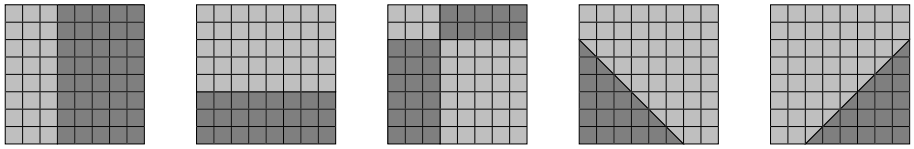

Figure 2: Four elementary families of cuts: (a) vertical, (b) horizontal, (c) checkerboard, (d), (e) oblique

The suggested refinement may also consist in dividing the domain in four zones of different transmissivities like in Fig. 3. Then discontinuities between values of transmissivity

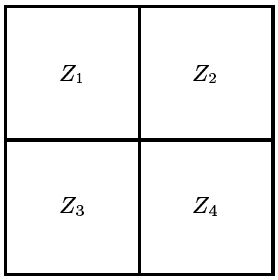

Figure 3: A four zone parameterization partition

in different zones can be written:

$$\sigma_{1,2} = T_1 - T_2, \quad \sigma_{2,4} = T_2 - T_4, \quad \sigma_{3,4} = T_3 - T_4, \quad \sigma_{1,3} = T_1 - T_3.$$

These four equations are not independent, as we have $\sigma_{1,2} - \sigma_{3,4} = \sigma_{1,3} - \sigma_{2,4}$. Therefore they correspond to only three independent constraints which we write as

$$\begin{array}{rcl} (T_1 + T_3) - (T_2 + T_4) & = & \sigma_V \\ (T_1 + T_2) - (T_3 + T_4) & = & \sigma_H \\ (T_1 + T_4) - (T_2 + T_3) & = & \sigma_C. \end{array} \tag{8}$$

The first equation (8) corresponds to a refinement given by a vertical line ($T_1 = T_3, T_2 = T_4$) dividing our domain into two zones. The second one corresponds to a horizontal cut ($T_1 = T_2, T_3 = T_4$) and the third one corresponds to a checkerboard cut ($T_1 = T_4, T_2 = T_3$). The matrix A corresponding to constraints (8), is now

$$A = \begin{bmatrix} 1 & -1 & 1 & -1 \\ 1 & 1 & -1 & -1 \\ 1 & -1 & -1 & 1 \end{bmatrix}.$$

Using the first equation in (5), we deduce that the associated Lagrange multiplier $\lambda^* = (\lambda_V^*, \lambda_H^*, \lambda_C)^*$ satisfies

$$\begin{array}{rcl} \lambda_V^* + \lambda_H^* + \lambda_C^* & = & \dfrac{\partial J}{\partial T_1}(T^*), \\ -\lambda_V^* + \lambda_H^* - \lambda_C^* & = & \dfrac{\partial J}{\partial T_2}(T^*), \\ \lambda_V^* - \lambda_H^* - \lambda_C^* & = & \dfrac{\partial J}{\partial T_3}(T^*), \\ -\lambda_V^* - \lambda_H^* + \lambda_C^* & = & \dfrac{\partial J}{\partial T_4}(T^*), \end{array} \tag{9}$$

where

$$0 = \frac{\partial J}{\partial T_1}(T^*) + \frac{\partial J}{\partial T_2}(T^*) + \frac{\partial J}{\partial T_3}(T^*) + \frac{\partial J}{\partial T_4}(T^*) = \frac{\partial J}{\partial T}(T^*) \tag{10}$$

since T^* is the minimizer for problem $(\mathcal{P}_1)$ where the parameter is constant over the whole domain. The refinement indicators λ_V^*, λ_H^* and λ_C^* associated respectively to the vertical, horizontal and checker board cuts are easily computed from formula (9) and (10).

So we see that in all cases, refinement indicators can be computed easily from the partial derivatives $\dfrac{\partial J}{\partial T_j}(T^*)$ of the misfit function with respect to transmissivities which are constant over some subzones of the current zonation. In practice, the optimal transmissivity T^* on the current zonation $\mathcal{Z}$ is computed by applying a gradient algorithm to the minimization of J.

Hence not only $T^* = (T^*{}_i, Z_i \in \mathcal{Z})$ are available, but also the partial derivatives $\dfrac{\partial J}{\partial T_i}(T^*), Z_i \in \mathcal{Z}$, which are equal to zero at a minimizer. The key is to compute these partial derivatives (i.e. the gradient of J for the current parameterization) by the adjoint approach which provides, at no additional cost, all the partial derivatives $\dfrac{\partial J}{\partial T_K}(T^*)$, where

K is the elementary cell or element of the discretization of the problem. Summing these elementary partial derivatives inside each zone of the current zonation $\mathcal{Z}$ provides the gradient of J which is required to run the minimization algorithm for the determination of T^*. But once T^* is calculated, summation of these $\dfrac{\partial J}{\partial T_K}(T^*)$ over all K inside any subzone of $\mathcal{Z}$ will provide, at almost no cost, the partial derivatives $\dfrac{\partial J}{\partial T_i}(T^*), Z_i \in \mathcal{Z}$ required for the determination of refinement indicators λ .
Hence the indicators λ associated to a large number of tentative cuts can be evaluated, and only the few with the largest absolute value are selected. The misfit function is then minimized for each of the refined parameterization obtained by implementing the cut corresponding to one of the selected indicators.

Finally, the refinement $\mathcal{Z}'$ of $\mathcal{Z}$ which corresponds to the cut providing the largest decrease of J is implemented. $\mathcal{Z}'$ has only one more degree of freedom than $\mathcal{Z}$, but produces a significant decrease of the objective function.

2.2 Coarsening indicators

Consider the example shown in Fig. 1, and suppose that in a first step the cut represented in Fig. 1(c) is selected: the partition $\mathcal{Z}$ contains two zones, an interior zone Z_1 and an exterior zone Z_2, with the corresponding optimal values of transmissivity T_1^* and T_2^*. Suppose that refinement indicators corresponding to various positions and forms of cuts have been computed and that two cuts C_1 and C_2 in the interior zone have been selected (Fig. 4 left), which both correspond to an indicator λ with a strong modulus. This indicates that there are two quite different ways of dividing the current interior zone Z_1 into two subzones, which each are likely to give a strong decrease to the least squares fit J. Rather than selecting arbitrarily one of these cuts, a natural thing would be to think of implementing them simultaneously, thus dividing the current interior Z_1 into three subzones $Z_{1,1}$, $Z_{1,2}$ and $Z_{1,3}$ (Figure 4, right), and hence adding two degrees of freedom to $\mathcal{Z}$.
But before choosing definitively this new zonation, one wants to make sure that the four degrees of freedom $Z_{1,1}$, $Z_{1,2}$, $Z_{1,3}$ and Z_2 are not overabundant. To do that, one checks whether the current discontinuity $T_1^* - T_2^*$ between Z_1 and Z_2 could be set to zero on some part of $\partial Z_1 \cap \partial Z_2$ without increasing the optimal misfit $J^*(T_1^*, T_2^*)$. Therefore we would like to define coarsening indicators $\lambda_j^*, j = 1, 2, 3$ such that the first order variation of J^* is given by $\Delta J_j^* = -\lambda_j^*(T_1^* - T_2^*), j = 1, 2, 3$. In order to do this we notice that minimizing the misfit function of two variables $J(T_1, T_2)$ over the current parametrization of Fig. 1(c)is equivalent, to minimizing $J(T_{1,1}, T_{1,2}, T_{1,3}, T_2)$, a function of four variables, over the parametrization of Fig. 4 right under the constraints

$$\begin{aligned} T_{1,1} - T_2 &= T_1^* - T_2^*, \\ T_{1,2} - T_2 &= T_1^* - T_2^*, \\ T_{1,3} - T_2 &= T_1^* - T_2^*. \end{aligned}$$

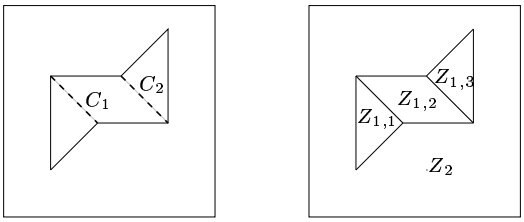

Figure 4: A refinement for Figure 1(c)

We can write these constraints in matrix form as

$$\begin{bmatrix} 1 & 0 & 0 & -1 \\ 0 & 1 & 0 & -1 \\ 0 & 0 & 1 & -1 \end{bmatrix} \begin{bmatrix} T_{1,1} \\ T_{1,2} \\ T_{1,3} \\ T_2 \end{bmatrix} = \begin{bmatrix} T_1^* - T_2^* \\ T_1^* - T_2^* \\ T_1^* - T_2^* \end{bmatrix}.$$

Aggregating for example the two zones Z_1^1 and Z_2 is equivalent to set to 0 the righthand side of the first constraint:

$$\begin{aligned} T_{1,1} - T_2 &= 0, \\ T_{1,2} - T_2 &= T_1^* - T_2^*, \\ T_{1,3} - T_2 &= T_1^* - T_2^*. \end{aligned}$$

The effect, at first order, of this aggregation on the optimal data misfit is measured by the corresponding Lagrange multiplier

$$\lambda_1^* = \frac{\partial J}{\partial T_{1,1}}(T_1^*, T_2^*).$$

Similarly the effects of aggregating $Z_{1,2}$ with Z_2 and $Z_{1,3}$ with Z_2 are measured respectively by

$$\lambda_2^* = \frac{\partial J}{\partial T_{1,2}}(T_1^*, T_2^*), \quad \lambda_3^* = \frac{\partial J}{\partial T_{1,3}}(T_1^*, T_2^*).$$

Notice that one has

$$\lambda_1^* + \lambda_2^* + \lambda_3^* = \frac{\partial J}{\partial T_1}(T_1^*, T_2^*) = -\frac{\partial J}{\partial T_2}(T_1^*, T_2^*) = 0. \tag{11}$$

Multiplying (11) by $T_1^* - T_2^*$ we see that

$$\Delta J_1^* + \Delta J_2^* + \Delta J_3^* = 0.$$

Hence one at least of the ΔJ_i^* is negative, so that aggregating the degrees of freedom $Z_{1,j}$ and Z_2 for which $\Delta J_i^* < 0$ will lower the number of degrees of freedom and enhance - at least at first order - the fit to the data. After this coarsening indicator step, the new zonation $\mathcal{Z}'$ will have only one more degree of freedom than $\mathcal{Z}$ (if only one of the ΔJ_j^* is negative), or even the same number of degrees of freedom (if two of the ΔJ_j^* are negative as this will be the case in the first numerical example below).

2.3 Algorithm

We have used the refinement and coarsening indicators introduced above, for several numerical studies according to the following algorithm:

1. Choose an initial parameterization partition $\mathcal{Z}$.
2. **Do** until data are satisfactorily fitted:
   3. Estimate the transmissivity with the current parameterization partition $\mathcal{Z}$ by minimizing J.
   4. **For** every zone Z_i of $\mathcal{Z}$ **do**

      Compute all the refinement indicators I corresponding to the chosen family of cuts.

      Enddo
   5. Compute I_{max} the largest absolute value of all computed refinement indicators in all parts Z_i. Select all cuts corresponding to refinement indicators which are larger than 80% of I_{max} (this percentage can be adjusted)
   6. **If** some of these cuts generate subdomains with more than one connected component **then**

      Compute the refinement indicators corresponding to the subcuts associated to each connected component (this will be the case each time checker board cut is selected!).
      Update the set of selected cuts according to the 80% rule.

      Endif
   7. **If** the selected cuts or a priori information suggest a refinement pattern to the user **then**

      Compute the corresponding refinement indicator, and update the set of selected cuts.

      Endif
   8. **If** two or more selected cuts divide the same part Z_i **then**

      Compute the corresponding coarsening indicators.
      Aggregate the subdomains where coarsening indicators allow it.

Endif

9. **If** there is at most one selected cut in each zone **then**

   Minimize J successively with all parameterizations associated to all selected cuts. Keep only the cut which induces the largest decrease of J

   Endif

10. Update the current partition according to the selected refinement or coarsening.

Enddo

Remark 1 *It is possible to skip step 7 and go directly to step 8 in order to obtain an automatic procedure. This will necessitate the calculation of a few extra coarsening indicators.*

3 Numerical experiments

3.1 Case of full observations

Numerical experiments have been performed in several simple situations. They correspond to synthetic examples in which we try to recover two or three transmissivity values and the zones where they take these values (the range of these values go from 5 to 20). In all examples boundary and initial data are zero and the righthand side Q of equation (1) is constant in space and time. The piezometric heads are measured in the whole domain and at all time.

3.1.1 Case of a central inclusion

We begin our numerical study by the case of a central inclusion (Fig. 5). We suppose that the initial transmissivity is constant in the whole domain (Fig. 6) and minimize the misfit function according to this parameterization. The different absolute values of refinement indicators are represented in Fig. 7. The largest values (flat part of the curve at its left) correspond to four checkerboard cuts, so we go to step 6 of the algorithm, and we compute the refinement indicators corresponding to corner subcuts of the checkerboard cuts (there are four corner subcuts for each checkerboard cut).

Four of these subcuts, represented by the symbols *, x, • and ∘, are selected, their geometry is shown in Figure 8, and the corresponding absolute value of the indicators are shown by the form *, x, • and ∘ symbols in Figure 7. Then we notice that Figure 8 suggests to "aggregate" the four corner cuts into a "rectangle cut", and, according to step 7 of the algorithm, we compute the corresponding refinement indicator (symbol □ on Fig. 7). We observe that it has the largest absolute value of all computed refinement indicators. Therefore we select it and we obtain at the end of this first iteration the partition shown in Fig. 9.

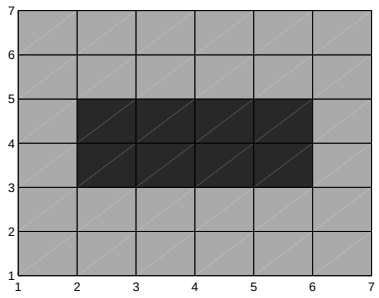

Figure 5: Exact transmissivity: unknown of the inverse problem

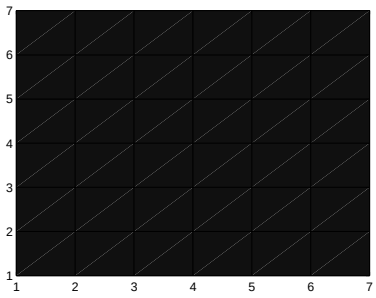

Figure 6: Initial transmissivity

For the second iteration we begin by minimizing the misfit function, considering the partition of Figure 9 obtained at the first iteration. This gives the two zone transmissivity shown in Figure 11. Then we compute again all refinement indicators in each zone and we observe that their highest absolute value corresponds to two cuts which divide the central zone into three parts (Fig.11). The three corresponding coarsening indicators are computed. Figure 10 shows that removing the transmissivity discontinuity between the exterior zone and both the top and bottom parts of the central zone will decrease the misfit function, which is not the case if we remove the transmissivity discontinuity between the middle part of the central zone and the exterior zone. Therefore only the middle part, is selected and we obtain the new partition shown in Fig. 12.

At the beginning of the third iteration, after minimization, the misfit function vanishes up to machine precision, with transmissity values that correspond to the exact ones (Fig. 13).

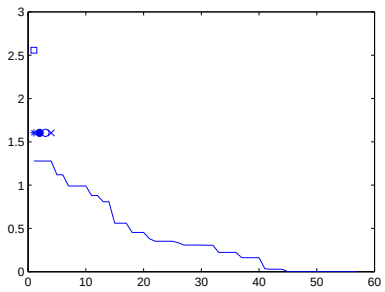

Figure 7: Computed absolute values of refinement indicators in decreasing order

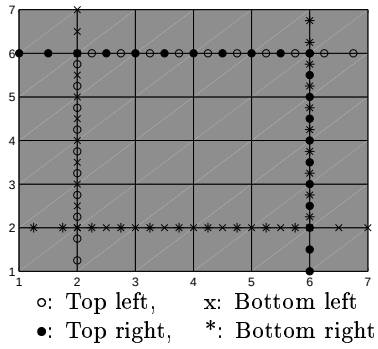

Figure 8: The 4 corner cuts corresponding to the largest absolute values of computed refinement indicators

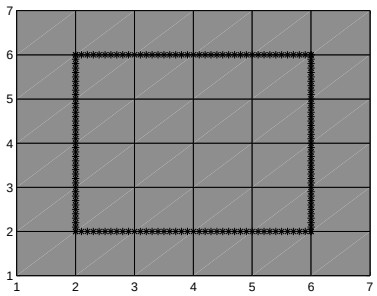

Figure 9: Partition obtained at the end of the first iteration

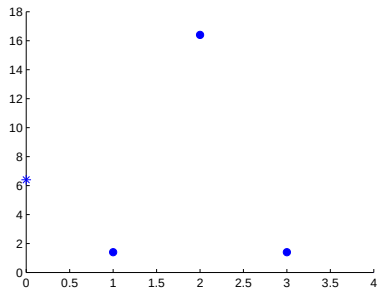

Figure 10: Values of the misfit function corresponding to the three computed coarsening indicators

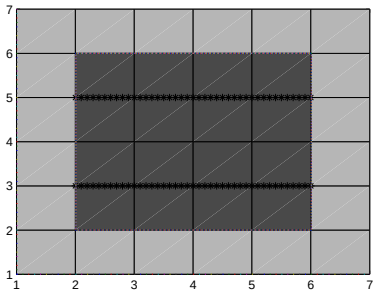

Figure 11: Computed transmissivity calculated on the partition shown in Fig. 9 and selected cuts

Let μ_i be the ith singular value of the Jacobian of Φ with respect to transmissivity parameters, the singular values being indexed with decreasing values, and let $\mu_{\max}$ be the largest of these singular values. The number of the singular values is equal to the number of zones in the zonation. To estimate the conditioning of the minimization problem we consider the ratio $\dfrac{\mu_i}{\mu_{\max}}$ which is plotted in Figure 14 for three cases with a logarithmic scale on the vertical axis. In the first two cases the constant initial transmissivity and the exact transmissivity are parameterized with one unknown per grid cell while in the third case the exact transmissivity is parameterized with the exact zonation represented in Figure 12. We observe that, as expected, the conditioning of the minimization problem is better when considering the two zone parameterization than when considering the one zone per grid cell parameterization. This demonstrates the interest of our algorithm which tries to minimize the number of zones used in the parameterization.

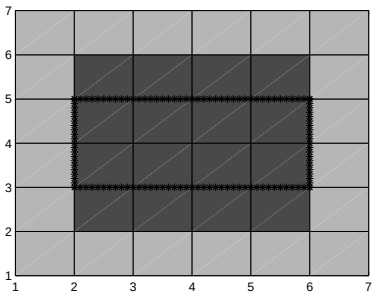

Figure 12: Partition obtained at the end of the second itération

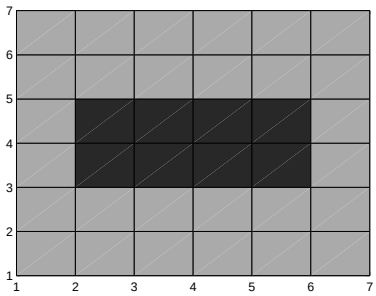

Figure 13: Optimal transmissivity computed with partition shown in fig. 12 is equal to the exact transmissivity

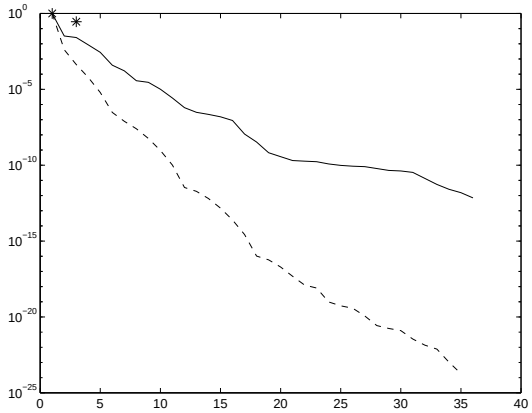

dotted line: constant initial transmissivity with one unknown per grid cell
continuous line: exact transmissivity with one unknown per grid cell
$*$: exact transmissivity with the exact two zone zonation in Fig. 13

Figure 14: Case of a centered inclusion: ratio $\frac{\mu_i}{\mu \max}$ as a function of i

We also tested the behaviour of the algorithm with respect to noise on the measured data. Even for high level of noise (80%) the true parametrization is recovered, thanks to using a larger number of optimization iterations and a larger final number of zones (see fig. 15). This good results may be credited to the fact that a complete observation, in both space and time, has been used to perform this inversion.

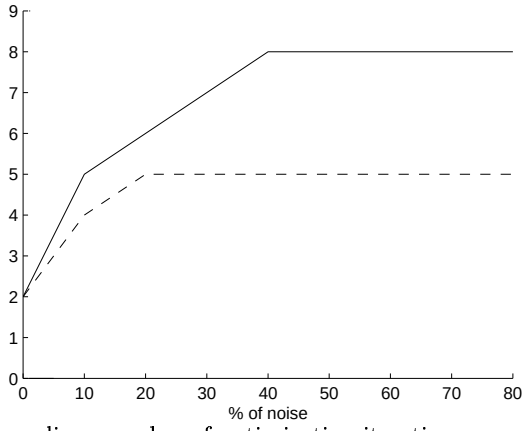

continuous line: number of optimization iterations
dotted line: number of estimated zones

Figure 15: Number of optimization iterations and number of estimated zones as functions of the noise level

3.1.2 Case of an off-centered inclusion

Now we consider the case of an off-centered inclusion (fig. 16). We start with the same constant initial transmissivity as in the previous case (fig. 6) and we proceed in the same manner. Figures 17, 18, 19, 20, 21 show the partitions obtained at each iteration and the transmissivity calculated on these partitions. We remark observing fig. 21 that the optimal transmissivity is recovered with four zones instead of two. Even though the number of zones (4) is not optimal, it is much smaller than the number of calculation cells (36), which again shows the interest of the method.

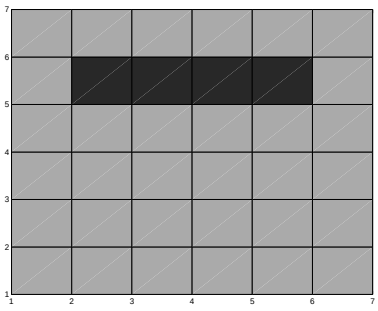

Figure 16: Exact transmissivity: unknown of the inverse problem

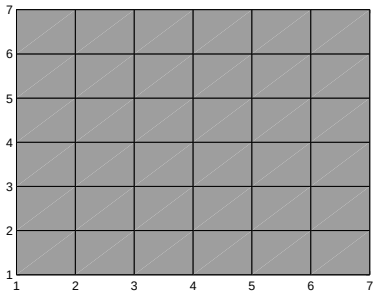

Figure 17: Transmissivity computed as a constant

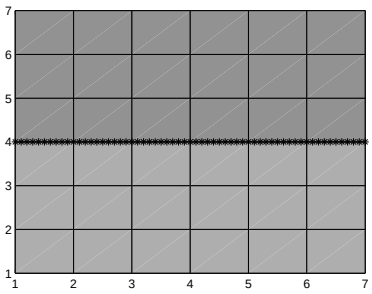

Figure 18: Partition obtained at the first iteration and the corresponding computed transmissivity

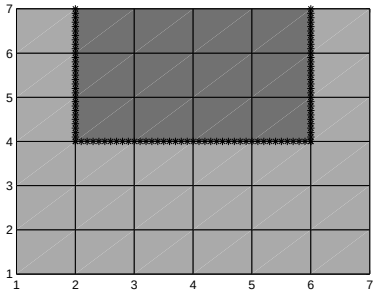

Figure 19: Partition obtained at the second iteration and the corresponding computed transmissivity

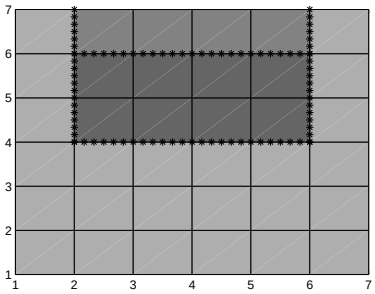

Figure 20: Partition obtained at the third iteration and the corresponding computed transmissivity

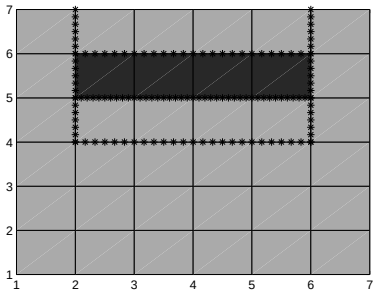

Figure 21: Partition obtained at the fourth iteration and the corresponding computed transmissivity

As for the case of a centered inclusion we evaluate the conditioning of the minimization problem by looking at the singular values μ_i of the Jacobian of Φ. From Fig. 22, we observe again that the the problem with the four estimated zones has a better conditioning than that using one zone per discretization cell.

At the third iteration, one could proceed in a way which departs from the algorithm presented in section 2.3 by considering, still using the selected cuts shown in Fig. 20, other partitions than that selected by the algorithm. Fig. 23 shows the two other partitions which can be considered. The optimal values of the misfit function corresponding to these two partitions are larger than that corresponding to the partition in Fig. 20, but the misfit function value corresponding to Fig. 23(b) is not much larger. Using this last partition, we continue the optimisation steps, and we compute the refinement indicators. Two cuts are then selected (Fig. 24). The optimal value of the misfit function is smaller in the case of the

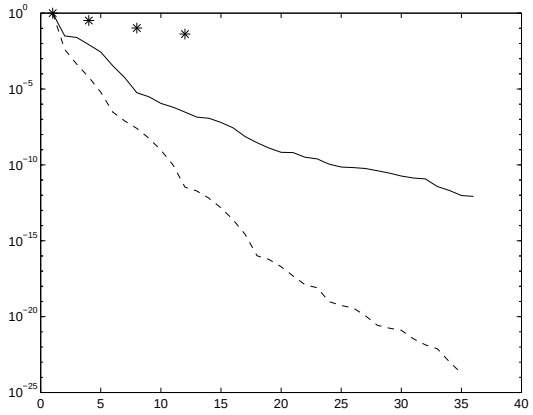

dotted line: constant initial transmissivity with one unknown per grid cell
continuous line: exact transmissivity with one unknown per grid cell
$*$: exact transmissivity with the exact four zone zonation in Fig. 21

Figure 22: Case of an off-centered inclusion: ratio $\frac{\mu_i}{\mu \max}$ as a function of i

top cut, so we obtain the partition in Fig. 25 with three zones of transmissivity instead of four as in Figure 21. Thus by allowing a small increase of the misfit function we obtain a better final zonation.

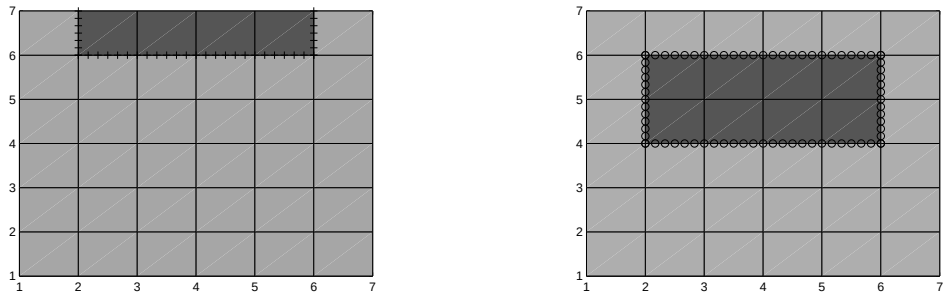

Figure 23: Other possible partitions that can be considered at the third iteration

We have plotted in Fig. 26 the singular value ratio $\frac{\mu_i}{\mu \max}$ obtained at the third and fourth iterations for both the regular algorithm (stars) and the above variant (circles). We

see that, surprisingly, the final three-zone parameterization obtained with the variant of the algorithm gives a slightly worse conditioning that the four-zone partition given by the regular algorithm.

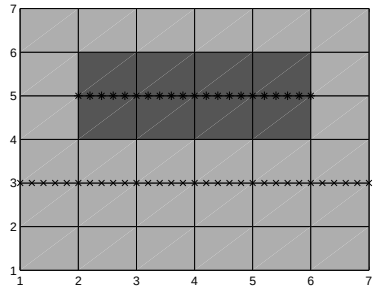

Figure 24: Cuts corresponding to the largest absolute values of the computed refinement indicators

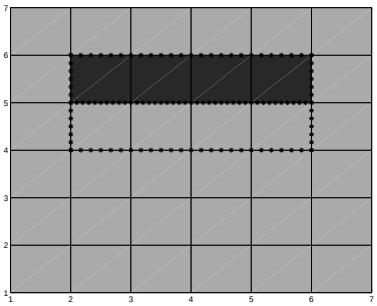

Figure 25: Estimated partition and transmissivity obtained when using a variant of the algorithm

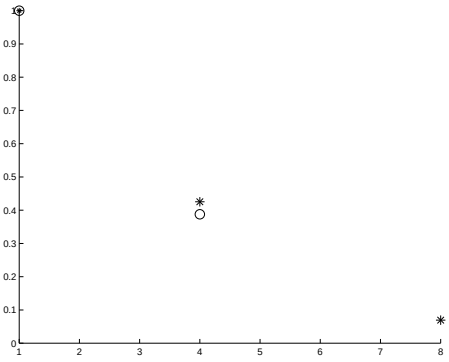

Third iteration

$*$: partition in Fig. 20
o: partition in Fig. 23 (b)

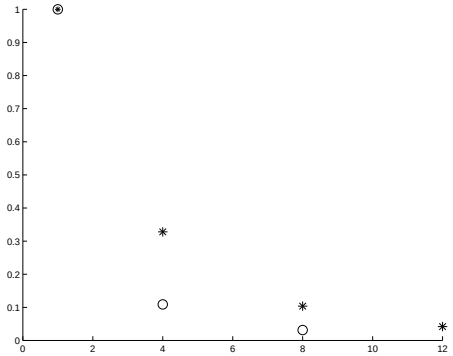

Fourth iteration

$*$: partition in Fig. 21
o: partition in Fig. 25

Figure 26: Ratio $\frac{\mu_i}{\mu_{\max}}$ as a function of i for partitions shown in Figs. 20 and 23 (b) for iterations 3 and 4 using the algorithm or a variant of it

3.1.3 A three-zone case

The last case that we consider is shown in Fig. 27. There are three zones of constant transmissivity, with a more complicated partition than that considered in the previous cases. One of these zones is the union of the two dark disjoint rectangles in Fig. 27. We start once again with a constant transmissivity (Fig. 6) and we follow the steps of the algorithm described in section 2.3. We show the successive partitions obtained at each iteration and the transmissivity computed on these partitions in Figures 28, 29, 30, 31, 32, 33, 34, 35, 36, 37, 38 and 39. In this last figure the estimated partition has 6 zones. Note that, on these figures, there is a drawing artefact because the drawing program that we used can represent only constant values on rectangles and therefore cannot properly represent oblique cuts.

We observe that, like in the previous case, only a close approximation of the exact partition and of the transmissivity values is recovered, but at all iterations the number of zones is very small compared to that of the cells of the computing mesh.

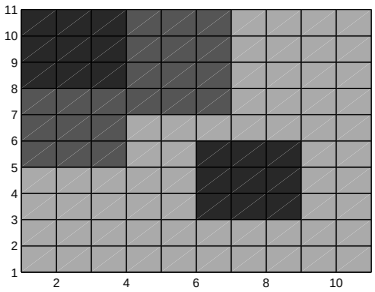

Figure 27: Exact transmissivity: unknown of the inverse problem

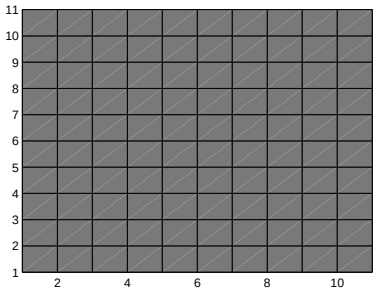

Figure 28: Transmissivity computed as a constant

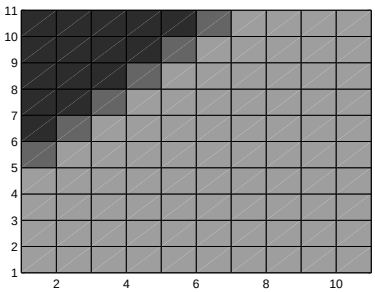

Figure 29: Partition obtained at the second iteration and the corresponding computed transmissivity

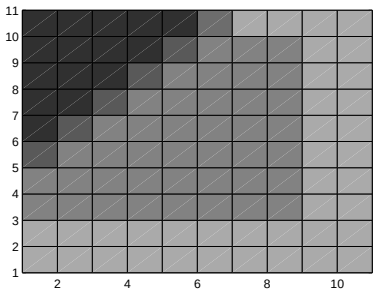

Figure 30: Partition obtained at the third iteration and the corresponding computed transmissivity

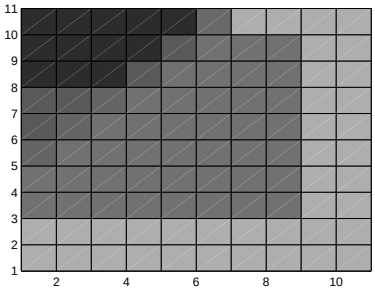

Figure 31: Partition obtained at the fourth iteration and the corresponding computed transmissivity

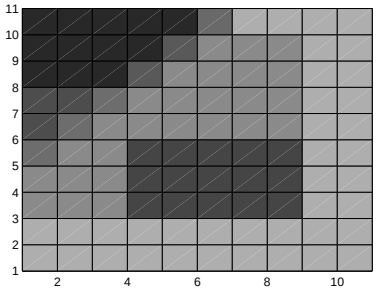

Figure 32: Partition obtained at the fifth iteration and the corresponding computed transmissivity

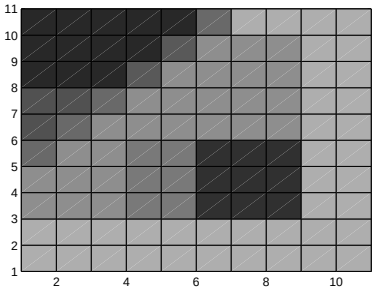

Figure 33: Partition obtained at the sixth iteration and the corresponding computed transmissivity

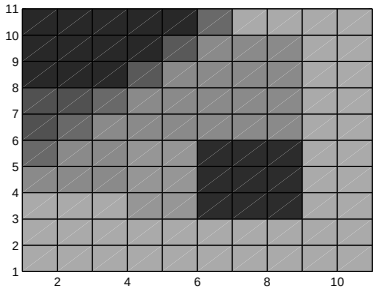

Figure 34: Partition obtained at the seventh iteration and the corresponding computed transmissivity

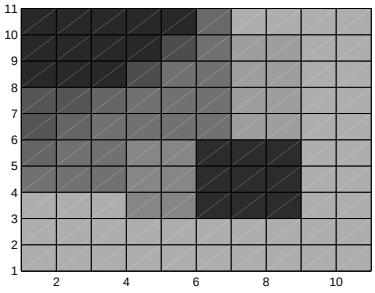

Figure 35: Partition obtained at the eighth iteration and the corresponding computed transmissivity

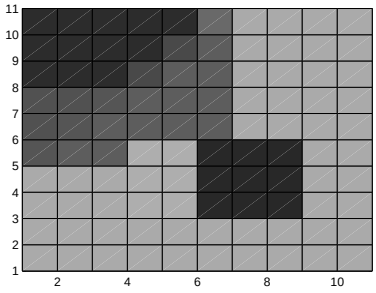

Figure 36: Partition obtained at the ninth iteration and the corresponding computed transmissivity

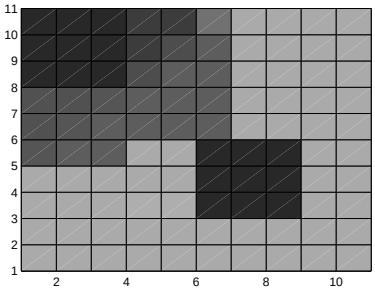

Figure 37: Partition obtained at the tenth iteration and the corresponding computed transmissivity

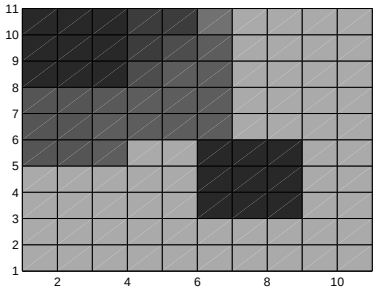

Figure 38: Partition obtained at the eleventh iteration and the corresponding computed transmissivity

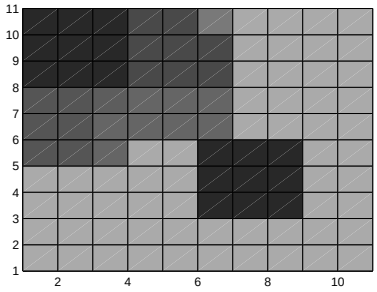

Figure 39: Partition obtained at the twelfth iteration and the corresponding computed transmissivity

Figure 40 shows that the conditioning of our problem is much improved when considering the parameterization obtained by our algorithm (Fig. 39, 6 zones) compared to the parameterization where the transmissivity zones are the calculation cells (100 zones).

3.2 Comparisons with other methods

We still consider the three-zone case of Fig. 27, with the same data, distributed in space and time.

We first compare with the standard method searching for one unknown per grid cell. In the noise free situation considered above, this method manages to retrieve the transmissivity pattern of Fig. 27. However, the total computation time required by the standard method to achieve convergence is seven times that required to perform the twelve refinement/coarsening steps described in the previous section (Figures 28 through 39). In terms of conditioning of

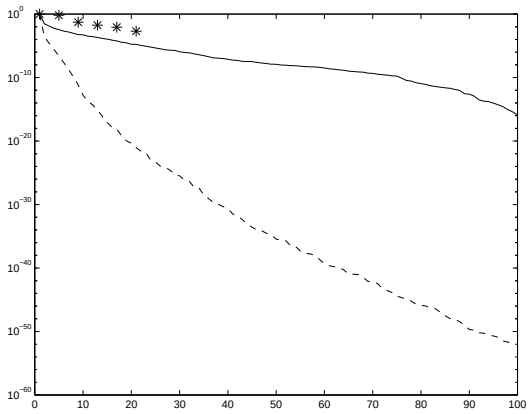

dotted line: constant initial transmissivity with one unknown per grid cell
continuous line: exact transmissivity with one unknown per grid cell
$*$: estimated transmissivity with the zonation shown in Fig. 39

Figure 40: Case of the three-zone zonation: ratio $\frac{\mu_i}{\mu \max}$ as a function of i

the final optimization problems, which indicates the stability level if noisy data were to be used, Fig. 40 shows the corresponding ratio of singular values $\mu_i/\mu_{\max}$. The conditionning for our adaptive parameterization is of the order of 10^{-3}, to be compared to 10^{-16} for the parameterization with one unknown per cell.

We compare now our adaptive parameterization to the multiscale parameterization [Liu, 1993, Chavent-Liu, 1989, Grimstadt et al., 2000, Yoon et al., 2000] where, at each step, regions of constant transmissivities are divided into four. After four such divisions (see Figs. 41, 42, 43, 44) the multiscale algorithm produces the 64 zones of constant transmissivities shown in Fig. 44, which is still far from the true values, despite the larger number of unknowns. If one performs one more division, the multiscale parametrization produces the same discretization as obtained with one unknown per grid cell. Hence in this example, the multiscale parameterization fails to reduce the number of unknowns required to explain the data, and is more computationaly intensive that our adaptive refinement technique.

3.3 Influence of the number of observations

We investigate now the behaviour of our algorithm in the more realistic situation where only partial measurements of the piezometric head are available. We still consider the three zone case of Fig. 27.

We first kept one measurement point in each grid cell, but decreased the time sampling of the data. This had little effect on the behaviour of the algorithm, which was able to

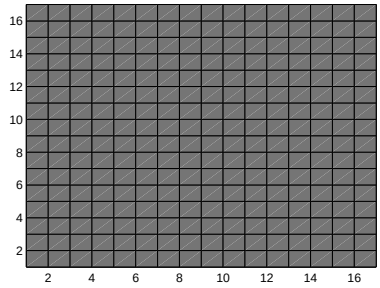

Figure 41: Computed transmissivity with a one zone parameterization

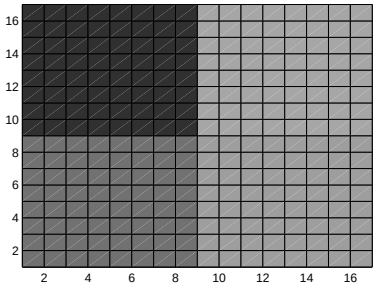

Figure 42: Computed transmissivity with a four zone parameterization

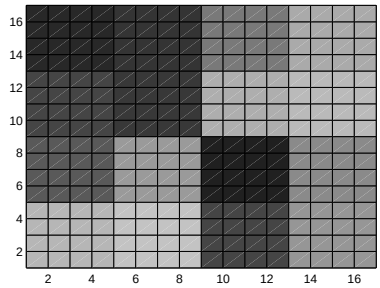

Figure 43: Computed transmissivity with a 16 zone parameterization

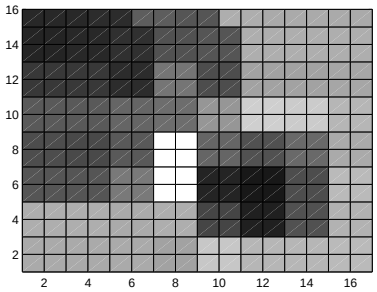

Figure 44: Computed transmissivity with a 64 zone parameterization

retrieve the true transmissivities, as long as more than 3 measures, evenly distributed in time, were available at each grid cell.

Then we returned to measurements at each time step, but decreased the number of observation points, as shown in Figures 45 (one measure in every other cell) and 47 (one measure in every fourth cell). In order to allow for comparison of the fit to the data achieved with different numbers of observation points, we evaluate this fit as

$$\text{Percentage of data explained} = 1 - \left(\frac{\sum_{i,j} |\Phi(T; x_j, t_i) - \Phi^m_{i,j}|^2}{\sum_{i,j} |\Phi^m_{i,j}|^2} \right)^{\frac{1}{2}} .$$

In the previous case of a full observation (one per cell), the final permeability distribution of Fig. 39 explained 99% of the data.

In the case of the observations of Fig. 45, the algorithm of section 2.3 produces, after eight refinement/coarsening steps, the the transmissivity distribution of Fig. 46, which explains 98% of the data. It is still quite close to that obtained with a full observation (Fig. 39), with some zones even correctly retrieved.

In the case of the observations of Fig 47, where only 25 measurement points are available, the same algorithm generates the distribution of Fig. 48, which explains 89% of the data. As one could expect, it is less detailed than the true distribution, and reproduces only its general trend, using only a small number of parameters.

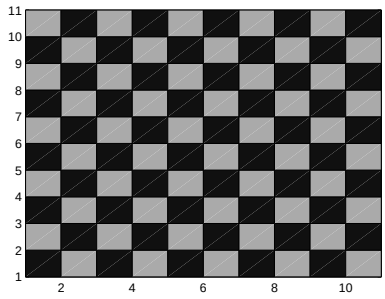

Figure 45: Dark cells: location of observations

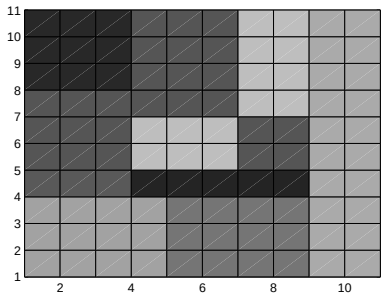

Figure 46: Computed transmissivity

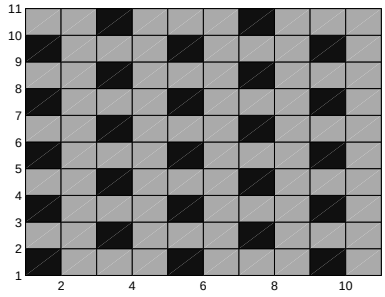

Figure 47: Dark cells: location of observations

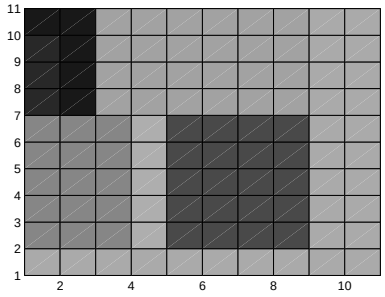

Figure 48: Computed transmissivity

Finally, we checked the effect of adding noise to the data in the last experiment. With a noise level of 10%, the algorithm produces the same parameterization as in absence of noise (Fig. 48), but at each step the refinement indicators decrease more slowly, which leads to select a larger number of cuts in step 5 of the algorithm according to the 80% rule, and hence to test a larger number of cuts in step 9. When the noise level is increased to 20%, the algorithm fails to retrieve the true distribution.

4 Conclusion

We presented an adaptive parameterization algorithm for estimating functions which are piecewise constant on an unknown zonation. At each refinement step, this algorithm

- ranks new potential degrees of freedom accordingly to their first order effect on the optimal data misfit using refinements indicators,
- nominates those with the largest refinement indicators,
- eventuallyy aggregates some of the nominated degrees of freedom with current ones using coarsening indicators,
- selects, among the remaining nominated degrees of freedom, that which gives the best actual decrease to the data misfit function.

The method has been tested on synthetic data with increasing complexity, with full or partial observation, possibly in the presence of noise.

It has shown its ability to determine both

- a partition of the domain in zones,
- a constant value in each zone,

which are consistant with the available data. The way the degrees of freedom are introduced have ensured in all cases that the final number of zones - and hence of parameters - was close to that used to generate the data, and small compared to the number of grid cells.

On the considered examples, it outperformed in terms of computation time and conditioning the parameterization with one degree of freedom per cell and the multiscale parameterization.

References

References

[Bonnans et al., 1997] J.F. Bonnans, J.-Ch. Gilbert, C. Lemaréchal, and C. Sagastizabal. *Optimisation Numérique Aspects théoriques et pratiques.* Springer-Verlag, 1997.

[Chardaire-Rivière et al., 1990] C. Chardaire-Rivière, G. Chavent, Jérôme Jaffré, and J. Liu. Multiscale representation for simultaneous estimation of relative permeabilities and capillary pressure, paper SPE 20501. In *65th Annual Technical Conference and Exhibition of the Society of Petroleum Engineers, New Orleans, Louisiana, September 23-26, 1990*, pages 303–312. Society of Petroleum Engineers, Richardson, Texas.

[Chardighy et al., 1996] E. Chardigny, P. Siegel, R. Mosé, and Ph. Ackerer. Parameter identification for complex groundwater systems. In A. Aldama and al., eds, *Computational Methods in Water Resources XI, Cancun, Mexico, July 22-26, 1996*, pages 305–312. Computational Mechanics Publications.

[Chavent, 1974] G. Chavent. Identification of functional parameter in partial differential equations In R.E. Goodson and M. Polis, eds, *Identification of Parameters in Distributed Systems*, ASME, 1974, pages 31–48.

[Chavent-Bissel, 1998] G. Chavent and R. Bissell. Indicator for the refinement of parametrization. In M. Tanaka and G.S. Dulikravich eds., *Inverse Problems in Engineering Mechanics*, Elsevier, 1998, pages 309–314.

[Chavent et al., 1994] G. Chavent, C. Chardaire-Rivière and J. Zhang. Estimation of mobilities and capillary pressure from centrifuge experiments In H.D. Bui et al. eds., *Inverse Problems in Engineering Mechanics*, A.A. Balkema, Rotterdam, 1998, pages 265–272.

[Chavent-Jaffré-Jégou, 1999] G. Chavent, J. Jaffré and S. Jegou. Estimation of relative permeabilities in three-phase flow in porous media. *Inverse Problems*, 15:33–39, 1999.

[Chavent-Liu, 1989] G. Chavent and J. Liu. Multiscale parametrization for the estimation of a diffusion coefficient in elliptic and parabolic problems. In A. El Jai and M. Amouroux, eds, *5th IFAC Symposium on Control of Distributed Parameter Systems, Perpignan, June 26-29, 1989*, Université de Perpignan, France, pages 315–324.

[Chavent-Roberts, 1997] G. Chavent and J. Roberts. A unified physical presentation of mixed, mixed hybrid finite elements and standard finite differences approximations of the determination of velocities in waterflow problems. *Advances in Water Ressources*, 14:326–348, 1997.

[Eppstein-Dougherty, 1996] M.J. Eppstein and D.E. Dougherty. Simultaneous estimation of transmissivity values and zonation. *Water Resources Research*, 32:3321–3336, 1996.

[Grimstadt et al., 2000] A.-A. Grimstadt, T. Mannseth, J.-E. Nordvedt, and G. Nævdal. Scale splitting can reduce cost and complexity of reservoir characterization Extended abstract in *Proc. 62nd EAGE Conference and Exhibition, Glasglow, 2000.*

[Jegou, 1997] S. Jegou. Using Maple for symbolic differentiation to solve inverse problems. *Maple Tech*, 4:32–40, 1997.

[Liu, 1993] J. Liu. A multiresolution method for distributed parameter estimation. *SIAM J. Sci. Comput*, 14:389–405, 1993.

[Sun, 1994] N.Z. Sun. *Inverse Problems in Groundwater Modeling.* Kluwer Academic Publishers, 1994.

[Yoon et al., 2000] S. Yoon, A. H. Malallah, A. Datta-Gupta, D. W. Vasco, and R.A. Behrens. A multiscale approach to production data integration using streamline models, Paper SPE 56653 in *1999 SPE Annual Technical Conference and Exhibition*. Society of Petroleum Engineers, October 1999.

Unité de recherche INRIA Rocquencourt
Domaine de Voluceau - Rocquencourt - BP 105 - 78153 Le Chesnay Cedex (France)

Unité de recherche INRIA Lorraine : LORIA, Technopôle de Nancy-Brabois - Campus scientifique
615, rue du Jardin Botanique - BP 101 - 54602 Villers-lès-Nancy Cedex (France)
Unité de recherche INRIA Rennes : IRISA, Campus universitaire de Beaulieu - 35042 Rennes Cedex (France)
Unité de recherche INRIA Rhône-Alpes : 655, avenue de l'Europe - 38330 Montbonnot-St-Martin (France)
Unité de recherche INRIA Sophia Antipolis : 2004, route des Lucioles - BP 93 - 06902 Sophia Antipolis Cedex (France)

Éditeur
INRIA - Domaine de Voluceau - Rocquencourt, BP 105 - 78153 Le Chesnay Cedex (France)
http://www.inria.fr
ISSN 0249-6399